Hybrid Assessment of Foot Arch Deformities Using Heatmap-Augmented Harris Mat Analysis and Morphometric Features

Abstract: *Arch type foot pathologies of Pes Cavus (high arch), Pes Planus (flatfoot), and normal arch patterns are good predictors of foot health that affect gait, posture, and predispose to musculoskeletal disorders. The research work described herein advances a computer-assisted automated classification of the foot arch from footprint images obtained on the Harris mat and transformed into pressure heatmaps, annotated by using machine learning classifiers, i.e., Support Vector Machines (SVM) and Convolutional Neural Networks (CNN). The system's performance was validated by testing on 300 images and was found to be extremely accurate in diagnosing. The total accuracy for the CNN model was 92%, with F1-score by class of 0.927 for Pes Cavus, 0.878 for Pes Planus, and 0.947 for Normal Arch. Precision values were 0.905 (Pes Cavus), 0.857 (Pes Planus), and 1 (Normal Arch), and recall values were 0.95, 0.90, and 0.90 respectively. The SVM model had an accuracy of 88%. Cohen's Kappa of 0.875 reflected almost perfect observer agreement, and ROC analysis revealed outstanding classification performance with AUC estimates of 0.95 for Pes Cavus, 0.91 for Pes Planus, and 0.95 for Normal Arch. Not only does the system yield correct foot arch classification, but it also has the potential to be applied to clinical practice, as a low-cost, cost-effective method for early detection and continuing monitoring of foot abnormalities in clinical and community health practice.*

Keywords: Harris mat, heatmap visualization, machine learning, automated diagnosis, footprint classification

INTRODUCTION

The intensity levels found in plantar pressure maps depend on both foot anatomy and the movement patterns and weight distribution of the body. [19] Traditional methods used for acquiring these distributions include Pedobarographs together with force plates.[13] The hardware systems used for static imprint analysis have limited scope of data collection[5] because they lack the ability to recreate past data obtained from Harris mat impressions. Images serve as an effective solution to show footprints yet pixel intensity lacks precision because it does not directly measure biomechanical pressures [2].

The study described an approach for making plantar pressure maps using Harris mat footprint images as starting material. A proposed system performs computational modeling to evaluate foot structure weight transfer under expectations by analyzing force distribution instead of using grayscale values for pressure identification. Using OpenCV preprocessing combined with mathematical pressure modeling develops plantar loading diagrams which function as independent biological pressure measurements without actual sensors.

The determination of pressure zone relationships with pixel intensity values happens through experimental procedures employed by researchers during footprint pressure measurement. The existing pixel intensity mapping system produces inconsistent pressure zone data because it does not work effectively with imaging variations and varying foot shapes. The method employs Gaussian distributions to model three-foot regions [4] including heels and forefeet and arches while it produces detailed force distribution heat maps instead of standard image enhancement techniques.

The system performs geometric improvements on Harris mat images through an extraction process of essential anatomical characteristics to produce mathematical pressure heatmaps. Users can refer to pressure distribution visuals through a web-platform interface with this system. The method breaks dependency on direct sensor measurement without altering the biomechanically valid framework to calculate pressure estimation from footprints.

The fundamental assessment methodology for plantar pressure evaluation depends on force sensors [6] although improvements in technology have failed to alter this method and remain impractical for clinical and research applications. The static footprint analysis is broadly used but since it does not measure dynamic gait movements it fails to deliver sufficient gait examination capabilities. The assessment method using grayscale intensity values for pressure zone analysis yields variable outcomes leading to problems in generating standardized evaluations. The paper adopts computational modeling techniques to analyze foot pressure distributions without pressure sensors and provides accurate and accessible plantar pressure evaluation methods.

Machine learning technology in medical imaging applications demands new automatic methods which use data-based approaches and generate identical clinical results.[7][8] At present research scientists employ CNNs to study pressure images which operate on raw grayscale images independently of theoretical biomechanical modeling applications. Gaussian-based pressure modeling produces force distributions in the proposed approach because they replicate actual biomechanical principles instead of performing purely data-driven computations. [14][4] The improved methods allow the system to create pressure maps that stay efficient but also allow clinical interpretations in biological terms for research and medical applications.

The method enables great possibilities for adapting it to telemedicine applications alongside remote patient monitoring solutions. This model provides pressure estimations that do not need special hardware sensors which makes it practical for home-based foot evaluations before clinical assessment. [1] Users maintain accurate medical assessments through a real-time system that displays foot pressure distribution via a web interface. The research develops fundamental principles which will enable future progress regarding non-invasive foot assessment systems through the improvement of traditional pressure mapping methods and footprint analysis efficiency.

METHODOLOGY

Study

A diagnostic strategy was established that merges standard foot anthropometry measured with artificial intelligence methods to categorize three types of foot arches (Pes Planus and Normal Arch and Pes Cavus). Next 106 static footprint impressions from both feet of healthy young adults were obtained by utilizing a Harris mat during data collection. The images were then digitized and saved as PDFs while expanding the dataset to 300 images through data augmentation procedures involving random rotations and horizontal flips and Gaussian blurring to eliminate class imbalance issues.

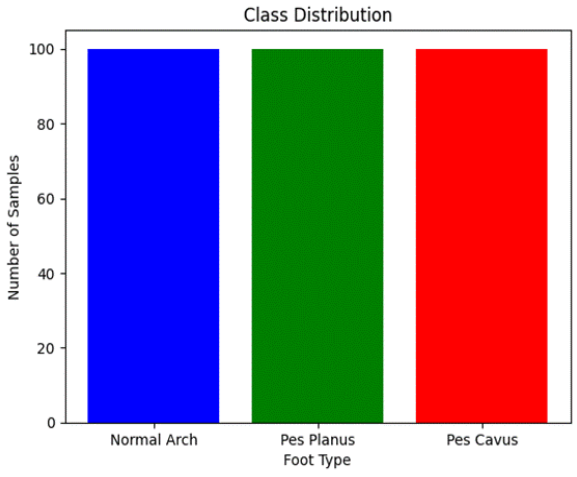

Fig 1. The foot type categories contain an approximately equivalent number of examples within Normal Arch, Pes Planus, and Pes Cavus classes.

Standard morphometric measures (Staheli and Chippaux-Smirak) and physiotherapist expert evaluations validated the obtained data. [10] All data received the appropriate anonymization Pes Planus (Flat Foot): Midfoot Width > 6.5 inches and increased arch-region intensity process before being secured in protected servers through standardized scanning protocols. [3] People with gait issues or previous injuries were not included in the study. [3] The trained classifiers based on rule-based methods and machine learning algorithms used the prepared dataset for determining important features that support clinical arch-type identification.

Data Preprocessing and Acquisition

Footprint images were obtained in PDF format through a standardized scanning procedure to maintain uniformity in all samples. The scanned footprints were then pre-processed through a custom-built preprocessing pipeline built in Python, utilizing PyMuPDF and OpenCV libraries. Each image was converted to grayscale and resized to 600×800 pixels to ensure dimensional uniformity. Binary thresholding was performed using Otsu's method to separate the footprint from the background. Next, the maximum contour was removed to determine the footprint boundary.

For anatomical alignment consistency throughout samples, Principal Component Analysis (PCA) was used to orient the foot so that the principal axis was in the vertical direction. [9] [22] This normalization allowed for accurate spatial comparison and region-specific analysis throughout the dataset.

Foot Region Segmentation and Index Calculation

Each aligned foot silhouette image was divided into three anatomical regions: the posterior 30% (heel), mid 30% (midfoot), and anterior 40% (forefoot) of the bounding box. [12] These areas were marked proportionally to the vertical size of the footprint.

For estimating plantar pressure distribution, binary images were smoothed using a Gaussian function and projected onto heatmaps according to the 'jet' colormap of Matplotlib. [4] The color intensities of the heatmap were employed as a surrogate measure for pressure magnitudes. [1][21]

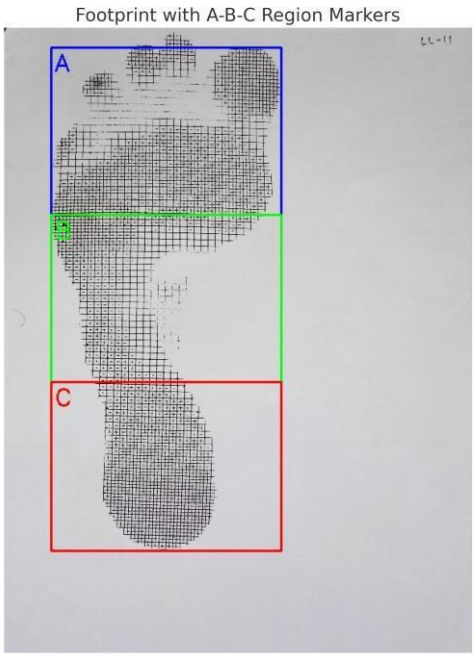

Fig 2. Analysis of the Arch Index depends on measurements taken in Areas A, B, C of the foot to determine structures within the forefoot, midfoot and hindfoot regions.

Quantitative morphometric measurements were computed for classification:

- Midfoot Width (MW): Narrowest width of the midfoot area
- Heel Width (HW): Widest width in the heel area
- Forefoot Width (FW): Maximum width in the forefoot area
-

Each pixel measurement was normalized to inches from DPI scaling. Two classic clinical indices were subsequently calculated:

- Staheli Index (SI):
  SI = Midfoot Width / Heel Width

- Chippaux-Smirak Index (CSI):
  CSI = (Midfoot Width / Forefoot Width)

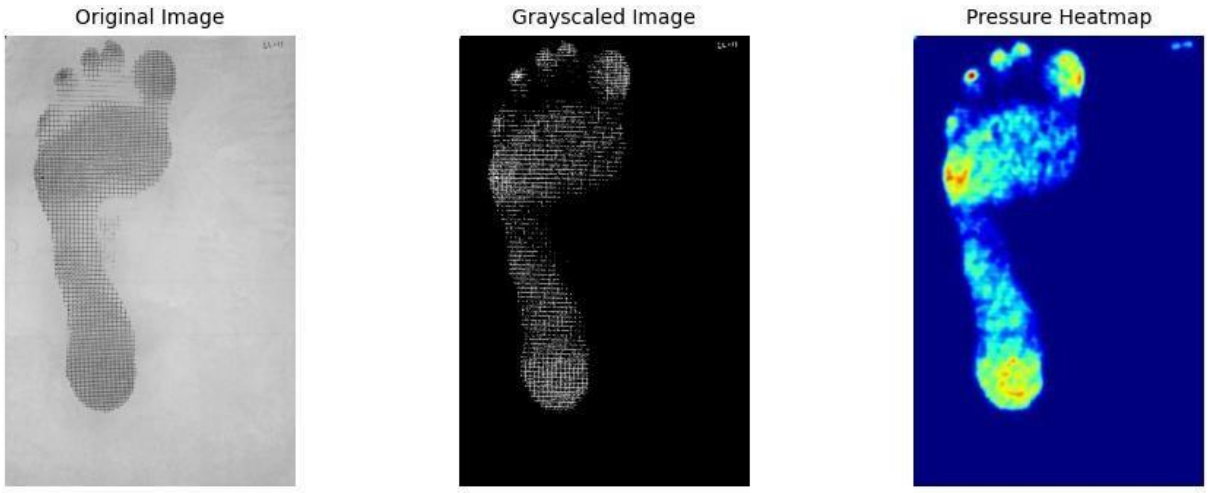

Fig 3. Arch classification analysis utilizes plantar pressure distribution which can be visualized through the combination of original baropodometric footprint images (left) and grayscale processing (center) and pressure heatmap (right).

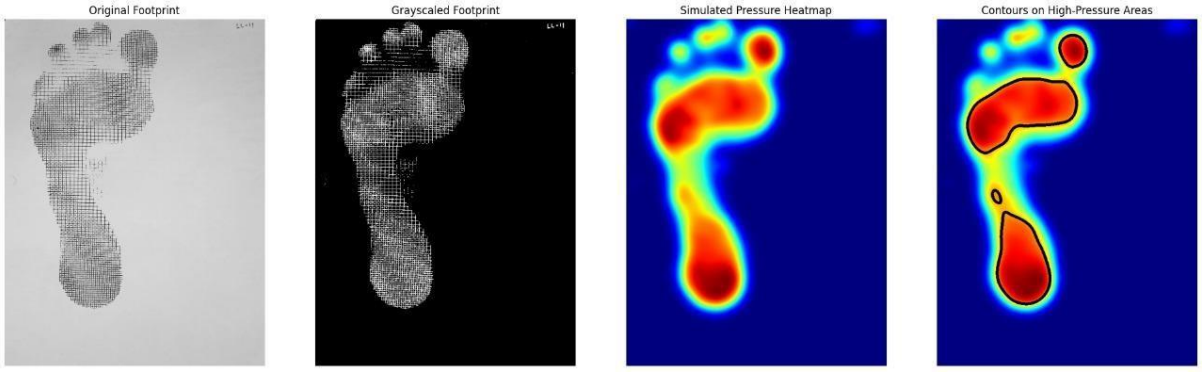

Fig 4. Sequential visualization of footprint analysis. The right column shows how the image evolves from a grayscale footprint, to a thresholded binary mask which leads to a Gaussian blur pressure heatmap followed by high-pressure contours placed on the heatmap.

Hybrid Rule-Based Classification

The hybrid rule-based classifier applied anatomical measures as well as regional intensity features derived from heatmaps. [6] Mean pixel intensity of the center 30% horizontal band (arch region) was computed after smoothing and normalization.

Empirically set thresholds were employed:

- Pes Planus (Flat Foot): Midfoot Width > 6.5 inches and increased arch-region intensity
- Pes Cavus (High Arch): Midfoot Width < 3.0 inches and low arch-region intensity
- Normal Arch: All other cases not falling under the above

The above method effectively integrated geometry and pressure simulation in diagnosis.[4][19] [20]
Besides the rule-based system, a Support Vector Machine (SVM) with a Radial Basis Function kernel and also a Convolutional Neural Network (CNN) on the MobileNetV2 architecture were trained. [9]
The dataset was augmented using random rotations (±15°), horizontal flipping, and Gaussian blur for robustness. [8] Stratified sampling was applied after augmentation to preserve class balance in training (240 images) and test (60 images) sets. [8] Data augmentation was only applied to the training set to prevent data leakage.
The CNN was learned using transfer learning and subsequently fine-tuned on the augmented data.[8][4][26] The SVM used handcrafted features derived from anatomical and intensity metrics.
System Integration and Web Deployment

A full stack web application was integrated with the classification pipeline [7]. A React frontend provided a responsive user experience for patients and physicians, while a Flask backend handled image ingestion, preprocessing, and model inference. Role authentication, raw and processed image thumbnails, annotated heatmap visualization, and longitudinal tracking for recurring users were among the features. Along with the indexes under "Foot Metrics" and lifestyle suggestions under "Recommendations" based on the kind of foot, the web application displays the patient's foot breadth and length (Fig 7c). It does so with a code integrated to the web application that calculates the foot length and width using dpi with accordance to the pixel size of the foot print found using OpenCV (cv2.minAreaRect() - a rotation-aware bounding box). The largest contour of the input is identified as footprint and longer side of rotated rectangle is classified as foot length and the shorter side as foot width, these values are converted from pixels to cm using dpi of the image.

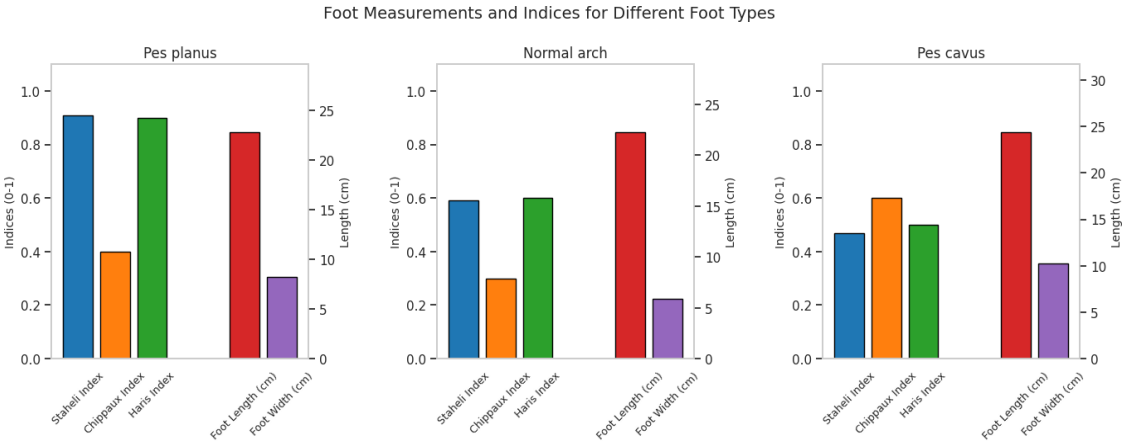

Fig. 5. Foot indices and measurements across Pes planus, Normal arch, and Pes cavus.

Table 1. Summary Statistics for Foot Arch Indices

Index	Mean	Std Dev	Median
Staheli Index	0.72	0.27	0.81
Chippaux Index	0.61	0.25	0.60
Haris Index	0.72	0.27	0.80

Table 2. Summary Statistics for Foot Measurements

Measurement	Mean	Std Dev	Median
Foot length (px)	1532.3	870.2	1509.0
Foot width (px)	551.2	284.6	541.5
Foot length (cm)	25.1	2.9	25
Foot width (cm)	9.5	1.4	9.5

Statistical Evaluation

Multi-class confusion matrix analysis was used to generate a set of established statistical metrics that were used for statistical analysis. Cohen's kappa coefficient, F1-score, accuracy, sensitivity (recall), specificity, precision, and the area under the Receiver Operating Characteristic curve (ROC-AUC) were among them. The purpose of these measurements was to give a thorough insight of overall system reliability as well as per-class diagnostic effectiveness.

The accuracy was measured by the number of correctly classified samples to that of all the predictions. Sensitivity (recall) was the system ability to detect all relevant examples for each type of foot arch, while specificity was the system ability to reject non-relevant samples. Accuracy was employed to determine the ratio of correct positive identifications to the total predictive positives. The F1-score, which is the harmonic mean of precision and recall, played a specific role in this setting because of the possibility of class imbalance where false positives and false negatives cannot be discarded. Cohen's kappas were computed to measure the agreement between predicted and actual classifications over that expected by chance, providing a robust inter-rater reliability measure in the multi-class case. Furthermore, ROC curves based on a one-vs-rest strategy were constructed for each class to plot sensitivity versus 1-specificity for different thresholds, and calculate ROC-AUC per model to measure the discriminating power of the same.

The CNN model's last test accuracy was 92% with a Cohen's kappa coefficient of 0.875, revealing an "almost perfect" agreement level. Class Specific F1-scores were 0.927, 0.878 and 0.947 for Pes Cavus, Pes Planus and Normal Arch, respectively, indicating high classification performance for all classes. One-vs-rest ROC-AUC was 0.95 for Pes Cavus, 0.9125 for Pes Planus, and 0.95 for Normal Arch, leading to a macro-average AUC equal to 0.93. These findings indicate that the discriminative ability of the CNN model was "very good," especially the reliability to detect both normal arch and flat arch patterns was very good.

As a baseline comparison, the support vector machine (SVM) model reached only 88% accuracy on the test set. While still competitive, the SVM look far less predictive than the CNN on all measures. The statistical analysis confirmed unanimously that the classification performance, and reliability, and sensitivity was better for the CNN compared to the SVM model especially for the multiclass foot arch shape detection.

RESULTS AND DISCUSSION

The rule-based hybrid classifier using morphometric features with intensity values based on heatmaps constituted a robust baseline with interpretable decision justification. This method, although straightforward, was successful at identifying clinically useful differences in pressure patterns and shape of footprint. This work proposed a strong and interpretable diagnosis framework for foot arch deformities namely Pes Planus, Pes Cavus, and Normal Arch using static footprint analysis. The pipeline successfully integrates traditional morphometric theory with contemporary machine learning techniques to ensure high diagnostic accuracy while remaining clinically interpretable.

Fig 6. A visual representation features Pes Planus in the middle while Normal Arch occupies the left section and Pes Cavus stands on the right to show structural variations between these classes.

The model's handling of the various diagnostic stages was made evident by metrics like accuracy, sensitivity, and F1 score. Out of all the parameters, recall (sensitivity) was used to gauge the model's ability to locate all of the positive examples, while precision was used to gauge how precise the model was in detecting those cases. The classifier's accuracy and the distribution of mistakes among Pes Planus, Pes Cavus, and Normal Arch were depicted in a comprehensive manner.

Model performance in avoiding incorrect classifications was assessed through the Specificity rate which gauges correct negative response ability. An F1-score was employed in this situation because it balances false negatives and false positives through calculating the harmonic mean between precision and recall statistics.

The evaluation included two metrics: overall accuracy allowed for correct measurement of identified samples among all predictions. The research included Cohen's Kappa coefficient to serve as a strong measure of inter-rater reliability which addressed accuracy limitations in multi-class classification problems when class distributions are unbalanced.

These measures formed an evaluation framework which effectively assessed data objectiveness and minority class response accuracy.

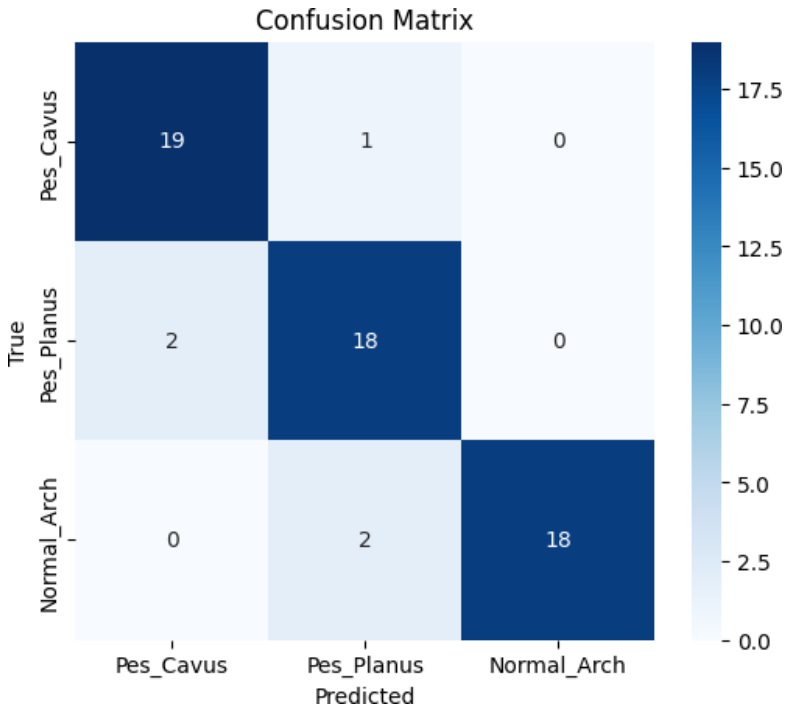

Fig 8. The classification model's performance evaluation shows misclassified instances scattered across all foot types within the confusion matrix

For the CNN model, the accuracy was 92%, with a Cohen's Kappa of 0.875, which is an inter-rater agreement of 'almost perfect'.
The class-wise F1 scores based on confusion matrix were 0.927 for Pes Cavus, 0.878 for Pes Planus and 0.947 for Normal Arch.

The test accuracy of the SVM model was 88%.

Table 3. Precision, accuracy, recall and f1 scores

Metric	Pes Cavus	Pes Planus	Normal Arch
Precision	0.905	0.857	1
Recall (Sensitivity)	0.95	0.90	0.900
F1 Score	0.927	0.878	0.947
Specificity	0.95	0.925	1

Overall Accuracy: 92%

Table 3. shows how the model performed for each category. The Arch model exceeded the metrics and achieved the highest possible scores. Even with the slight decrease, it is still possible to spot Pes Planus. That way, the model can notice slight distinctions in footprint shapes. Figure 9 indicates that the model is effective in separating high-risk from low-risk patients and correctly labeling unknown cases.

Fig 9. Precision, accuracy, recall and f1 scores comparison graphically

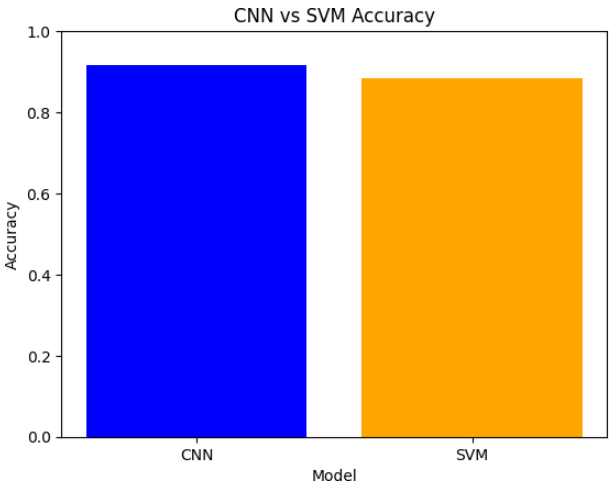

Fig 10. Accuracy comparison between CNN and SVM model

Additionally, Receiver Operating Characteristic (ROC) curves for all classes through a one-vs-rest approach were calculated. Area Under the Curve (AUC) values were 0.95 for Pes Cavus , 0.9125 for Pes Planus and 0.95 for Normal Arch.

The macro-average AUC was provided as:

AUC_macro = (0.95 + 0.9125 + 0.95) / 3 = **0.93**

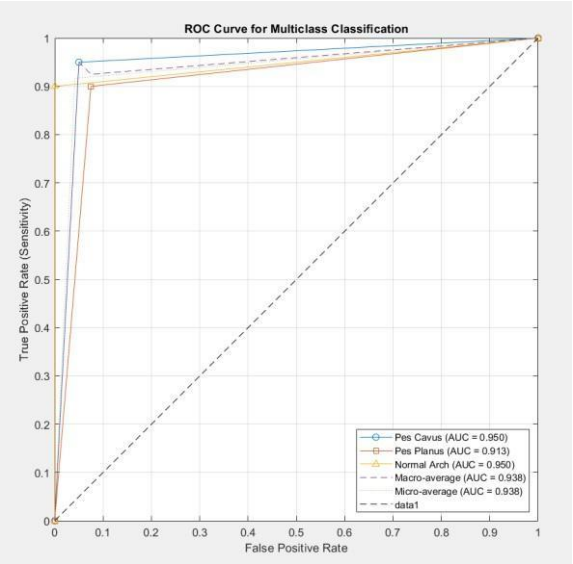

Fig 11. ROC curves plotted for each foot type evaluation group show how the model separates classes with effective true positive classification abilities.

These results indicate that the system works very well in discriminating between all three classes, particularly in the identification of flat and normal arches, and less sensitive in the identification of Pes Cavus.

Table 4. Receiver Operating Characteristic (ROC) and Area Under Curve (AUC) Analysis for Foot Arch Classification

Class	TPR	FPR	AUC Estimate
Pes Cavus	0.95	0.05	Around 0.95
Pes Planus	0.90	0.075	Around 0.91
Normal Arch	0.90	0	0.93-0.95

The data preprocessing pipeline provided consistent image quality and orientation throughout the data set. Applying Principal Component Analysis (PCA) to spatial normalizing and subdividing the footprint into anatomy regions, the task allowed region-of-interest analysis. Highly reliable-morphometric dimensions such as Midfoot Width (MW), Heel Width (HW), and Forefoot Width (FW) were responsible for clinically validated parameters such as Staheli Index (SI) and Chippaux-Smirak Index (CSI) determination.The hybrid classifier based on rules, which integrated these morphometric characteristics with intensity values as calculated from heatmaps, was a strong baseline with understandable decision logic. [24] This approach, although simple, proved potent in deriving clinically meaningful differences in footprint shape and pressure behaviours.

Parallel to this, the machine learning pipeline used both a Support Vector Machine (SVM) and a Convolutional Neural Network (CNN) based on MobileNetV2 architecture. The CNN, trained using transfer learning and fine-tuning with an augmented dataset, surpassed both SVM and rule-based classifiers with a test accuracy of 92% and Cohen's Kappa score of 0.875, which implies nearly perfect inter-rater agreement.

Per-class F1-scores of 0.878 for Pes Planus, 0.947 for Normal Arch, and 0.927 for Pes Cavus revealed sensitivity and accuracy across the three classes. Most surprisingly, Pes Planus was best recognized with confidence, most likely because of the uniqueness of anatomical and pressure characteristics of Pes Planus.[3][18]In contrast, Pes Cavus had somewhat smaller performance values due to the likelihood of morphological resemblance with Normal Arch class in some cases.

Receiver Operating Characteristic (ROC) analysis also supported the discriminative capability of the model with class-wise AUC scores of 0.9125 (Pes Planus), 0.95 (Normal Arch), and 0.95 (Pes Cavus), and a macro-average AUC score of 0.93.

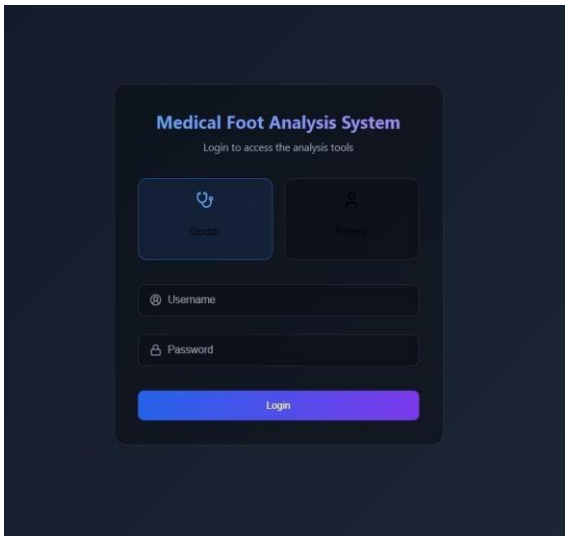

Fig 7a. Login Interface.

The system provides role-based authentication which grants clinicians and patients access to protected personal features.

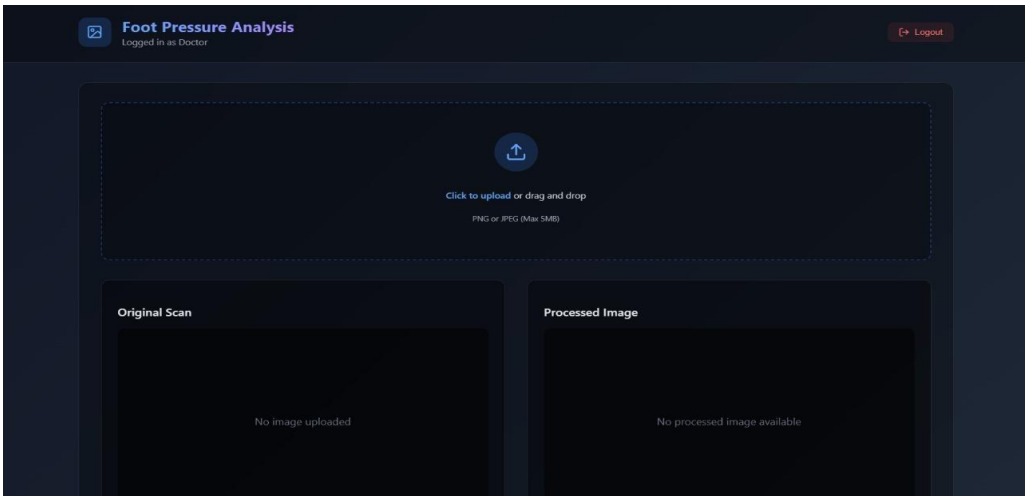

Fig 7b. Upload & Classification.

The system processes footprint images through uploaded and categorized views that display raw and processed images together.

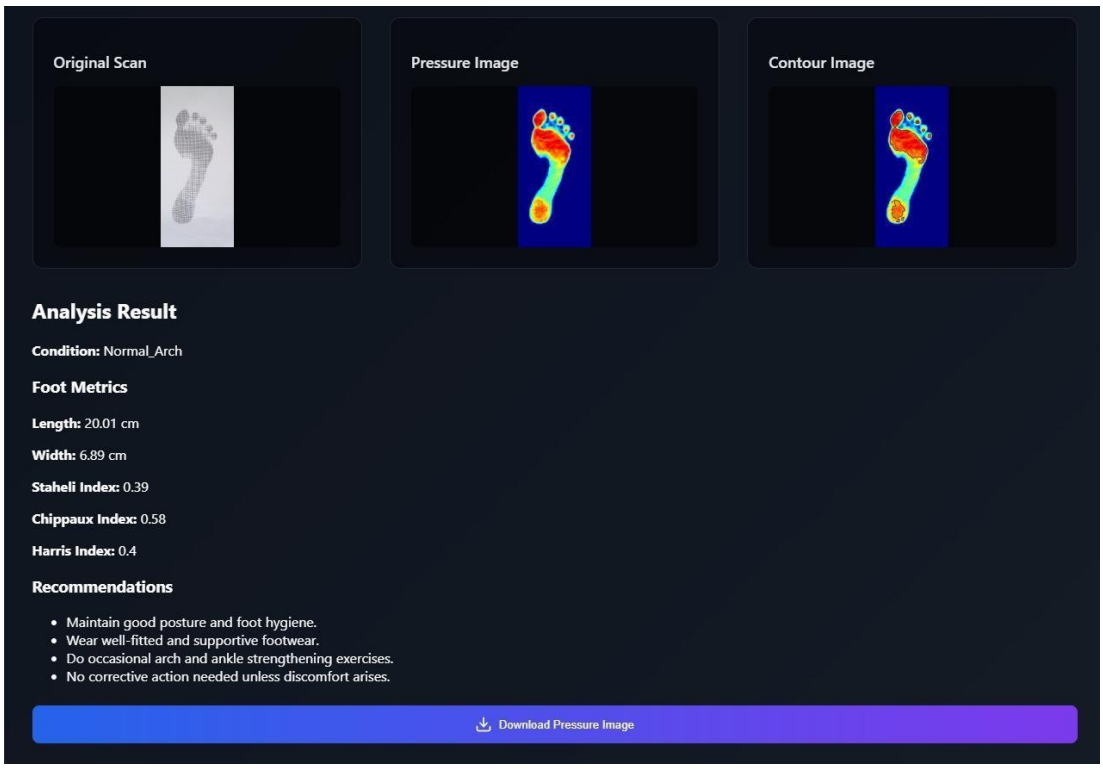

Fig 7c. Results & Recommendations.

The system shows a diagnosis provided by type with specific lifestyle advice presented in a approachable manner to patients.

The findings confirm the system to classify foot arch types accurately with high confidence. The integration of the entire classification pipeline into a Flask–React web application demonstrates its practical feasibility. [17] The accessibility of quantitative information and graphical heatmaps to clinicians and patient-friendly descriptions and lifestyle suggestions make the platform a useful resource for both medical practitioners and end-users.

CONCLUSION

This study introduces a new, hybrid diagnostic model which exploits morphometric feature extraction, simulated plantar pressure analysis, and machine learning classification to provide precise diagnosis of foot arch deformities from single footprint images. Combining rule-based logic anchored in clinical facts with current-state deep learning architectures ensures both interpretation and performance while filling the divide between classical diagnostics and contemporary AI systems.

The system showed 92% accuracy in classification with good generalization to all three target classes. The CNN model, facilitated by an optimally designed data preprocessing and augmentation pipeline, was most powerful. Its application in a web-based platform further accentuates its scalability, accessibility, and patient-focused diagnostic potential.

Future work will target improved diagnostic resolution using dynamic gait analysis, increased and more diverse data sets, and the addition of sensor-based biomechanical measurements. These enhancements will further enhance the clinical utility of the system as an accepted tool in preventive and rehabilitative podiatric practice.

REFERENCES

1. Babović, Siniša S, et al. "Labeling of Baropodometric Analysis Data Using Computer Vision Techniques in Classification of Foot Deformities." *Medicina*, vol. 59, no. 5, 26 Apr. 2023, pp. 840–840, https://doi.org/10.3390/medicina59050840. Accessed 10 Apr. 2025.
2. Cisneros, Lígia de Loiola, et al. "Inter- and Intra-Examiner Reliability of Footprint Pattern Analysis Obtained from Diabetics Using the Harris Mat." *Revista Brasileira de Fisioterapia (Sao Carlos (Sao Paulo, Brazil))*, vol. 14, no. 3, 2010, pp. 200–5, pubmed.ncbi.nlm.nih.gov/20730363/.
3. Açak, Mahmut. "The Effects of Individually Designed Insoles on Pes Planus Treatment." Scientific Reports, vol. 10, no. 1, 12 Nov. 2020, p. 19715, www.nature.com/articles/s41598-020-76767- y,https://doi.org/10.1038/s41598-020-76767-y.
4. Bai, Xiaotian, et al. "Plantar Pressure Classification and Feature Extraction Based on Multiple Fusion Algorithms." Scientific Reports, vol. 15, no. 1, 17 Apr. 2025, www.nature.com/articles/s41598-025-96440-6, https://doi.org/10.1038/s41598-025-96440-6. Accessed 3 May 2025.
5. Coughlin, Michael J., and Ari Kaz. "Correlation of Harris Mats, Physical Exam, Pictures, and Radiographic Measurements in Adult Flatfoot Deformity." *Foot & Ankle International*, vol. 30, no. 7, July 2009, pp. 604–612, https://doi.org/10.3113/fai.2009.0604.
6. Ghazaleh, Leila, et al. "Comparing Three Footprint Grades to Evaluate Footprint Indexes for Flat Foot Diagnosis." *Physical Treatments: Specific Physical Therapy Journal*, 30 Nov. 2019, pp. 137–146, https://doi.org/10.32598/ptj.9.3.137.
7. Gül, Yeliz, et al. "Artificial Intelligence Methodologies Applied to Technologies for Screening, Diagnosis and Care of the Diabetic Foot: A Narrative Review." Diagnostics, vol. 13, no. 9, 8 May 2023, p. 1662, mdpi-res.com/diagnostics/diagnostics-13-01662/article_deploy/diagnostics-13-01662.pdf?version=1683551720, https://doi.org/10.3390/diagnostics13091662. Accessed 14 Mar. 2024.
8. Deng, Yixiang, et al. "Deep Transfer Learning and Data Augmentation Improve Glucose Levels Prediction in Type 2 Diabetes Patients." NPJ Digital Medicine, vol. 4, no. 1, 14 July 2021, p. 109, pubmed.ncbi.nlm.nih.gov/34262114/, https://doi.org/10.1038/s41746-021-00480-x.
9. Lucas, Julien, et al. "Automated Spatial Pattern Analysis for Identification of Foot Arch Height from 2D Foot Prints." *Frontiers in Physiology*, vol. 9, 3 Sept. 2018, https://doi.org/10.3389/fphys.2018.01216. Accessed 16 Dec. 2019.
10. Siranya Paecharoen, et al. "Diagnostic Accuracy of Harris Imprint Index, Chippaux-Smirak Index, Staheli Index Compared with Talar-First Metatarsal Angle for Screening Arch of Foot." *Annals of Rehabilitation Medicine*, vol. 47, no. 3, 30 June 2023, pp. 222–227, doi.org/10.5535%2Farm.23015, https://doi.org/10.5535/arm.23015.
11. Siranya Paecharoen, and Thanutchaporn Kritsanapraneet. "Distribution of Foot Arch Type and Associated Symptoms in Medical Students at Faculty of Medicine, Thammasat University." *Deleted Journal*, vol. 76, no. 6, 1 June 2024, pp. 346–352, https://doi.org/10.33192/smj.v76i6.267251. Accessed 7 Aug. 2024.
12. Toyooka, Seikai, et al. "Validity of a Simple Footprint Assessment Board for Diagnosing the Severity of Flatfoot: A Prospective Cohort Study." *BMC Musculoskeletal Disorders*, vol. 22, no. 1, 18 Mar. 2021, pmc.ncbi.nlm.nih.gov/articles/PMC797727/, https://doi.org/10.1186/s12891-021-04154-3. Accessed 18 Apr. 2025.
13. Voronov, Michael L, et al. "Static Measure of Foot Loading." *Foot & Ankle Specialist*, vol. 2, no. 6, Dec. 2009, pp. 267–70, pubmed.ncbi.nlm.nih.gov/20400423/, https://doi.org/10.1177/1938640009349451.
14. Zhao, Yangyang, et al. "A Deep Learning Method for Foot-Type Classification Using Plantar

Pressure Images." *Frontiers in Bioengineering and Biotechnology*, vol. 11, 11 Sept. 2023,]https://doi.org/10.3389/fbioe.2023.1239246. Accessed 17 Nov. 2024.

15. Carr, James B, et al. "Pediatric Pes Planus: A State-of-the-Art Review." *Pediatrics*, vol. 137, no. 3, 2016, p. e20151230, www.ncbi.nlm.nih.gov/pubmed/26908688, https://doi.org/10.1542/peds.2015-1230. Accessed 11 Nov. 2019.
16. Chae, Jonghyeok, et al. "A Deep-Learning Approach for Foot-Type Classification Using Heterogeneous Pressure Data." *Sensors*, vol. 20, no. 16, 11 Aug. 2020, p. 4481, https://doi.org/10.3390/s20164481. Accessed 25 Nov. 2020.
17. Chevalier, Thierry L., and Nachiappan Chockalingam. "Effects of Foot Orthoses: How Important Is the Practitioner?" *Gait & Posture*, vol. 35, no. 3, Mar. 2012, pp. 383–388, https://doi.org/10.1016/j.gaitpost.2011.10.356. Accessed 27 Nov. 2021.
18. Choi, Jungkyu, et al. "Analysis of Pediatric Foot Disorders Using Decision Tree and Neural Networks." *2017 European Conference on Electrical Engineering and Computer Science (EECS)*, Nov. 2017, pp. 41–46, ieeexplore.ieee.org/abstract/document/8411993, https://doi.org/10.1109/eecs.2017.17. Accessed 16 May 2025.
19. Gwani, A. S., et al. "How the Three Arches of the Foot Intercorrelate." *Folia Morphologica*, vol. 76, no. 4, 2017, pp. 682–688, pubmed.ncbi.nlm.nih.gov/28553850/, https://doi.org/10.5603/FM.a2017.0049.
20. Kirby, Kevin A. "Longitudinal Arch Load-Sharing System of the Foot." *Revista Española de Podología*, vol. 28, no. 1, 1 Jan. 2017, pp. e18–e26, www.sciencedirect.com/science/article/pii/S0210123817300087#:~:text=Deep%20to%20the%20pl a ntar%20intrinsic, https://doi.org/10.1016/j.repod.2017.03.003.
21. Menz, Hylton B, et al. "Visual Categorisation of the Arch Index: A Simplified Measure of Foot Posture in Older People." *Journal of Foot and Ankle Research*, vol. 5, no. 1, 3 July 2012, jfootankleres.biomedcentral.com/articles/10.1186/1757-1146-5-10, https://doi.org/10.1186/1757-1146-5-10.
22. Nikolaidou, M.E., and K.D. Boudolos. "A Footprint-Based Approach for the Rational Classification of Foot Types in Young Schoolchildren." *The Foot*, vol. 16, no. 2, June 2006, pp. 82–90, https://doi.org/10.1016/j.foot.2006.02.001. Accessed 10 Oct. 2020.
23. Wang, Mo, et al. "Research on Feature Extraction Algorithm for Plantar Pressure Image and Gait Analysis in Stroke Patients." *Journal of Visual Communication and Image Representation*, vol. 58, Jan. 2019, pp. 525–531, https://doi.org/10.1016/j.jvcir.2018.12.017. Accessed 11 Oct. 2021.
24. Jung, Ji-Yong, et al. "Decision Tree-Based Foot Orthosis Prescription for Patients with Pes Planus." *International Journal of Environmental Research and Public Health*, vol. 19, no. 19, 30 Sept. 2022, pp. 12484–12484, pubmed.ncbi.nlm.nih.gov/36231782/, https://doi.org/10.3390/ijerph191912484. Accessed 11 Oct. 2024.
25. Banwell, Helen A, et al. "Foot Orthoses for Adults with Flexible Pes Planus: A Systematic Review." Journal of Foot and Ankle Research, vol. 7, no. 1, 5 Apr. 2014, https://doi.org/10.1186/1757-1146-7-23.
26. Danaci, Cagla, et al. "Diagnosis of Pes Planus from X-Ray Images: Enhanced Feature Selection with Deep Learning and Machine Learning Techniques." Biomedical Signal Processing and Control, vol. 106, 26 Feb. 2025, p. 107769, www.sciencedirect.com/science/article/abs/pii/S1746809425002800, https://doi.org/10.1016/j.bspc.2025.107769.